# GRMAG-1-12-360 core
## datasheet

**Grid Asset Performance > Next Generation Transformers**

The GRMAG-1-12-360 tape-wound core is manufactured with a custom iron-based metal amorphous nanocomposite. NASA Glenn Research Center (GRC) cast and fabricated the core. The ribbon is cast in a stanrdard 1” / 25 mm wide ribbon width and annealed with a transverse field for a square BH loop. While targeting a 10 kW, 20 kHz three port active bridge application this core material can generally be used for transformers, pulse power cores, motors, and high frequency inductors. The 12 and 360 in the name specify the $B_{sat}$ in T*10 and the low frequency permeability divided by 100, respectively.

**Date:** June 2019
Revision 0.2



*Fig. 1: Core under test (GRMAG-1-12-360).*

GRMAG-1-12-360 core

## Dimensions

*Table 1: Core dimensions.*

| Description | Value |
|---|---|
| H | 74mm |
| T | 8.5mm |
| G | 57mm |
| C | 16mm |
| W/2 | 33mm |
| W | 66mm |
| D/3 | 25.4mm (1 inch) |
| D | 76.2mm (3 inch) |

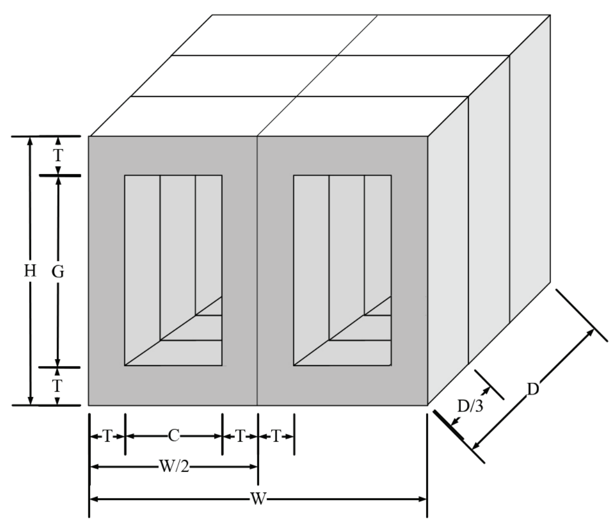


*Fig. 2: Illustration of core dimensions.*

**Acknowledgement**

This technical effort was performed in support of the National Energy Technology Laboratory's ongoing research in DOE's The Office of Electricity's (OE) Transformer Resilience and Advanced Components (TRAC) program under the RSS contract 89243318CFE000003.



NATIONAL ENERGY TECHNOLOGY LABORATORY

## Magnetic Characteristics

*Table 2: Magnetic characteristic.*

| Description | Symbol | Typical value | Unit |
|---|---|---|---|
| Effective area | $A_e$ | 10.152 | $mm^2$ |
| Mean magnetic path length[1] | $L_m$ | 168 | mm |
| Mass (before impregnation) | | 1.33025 | kg |
| Mass (after impregation) | | 1.364 | kg |

## Measurement Setup

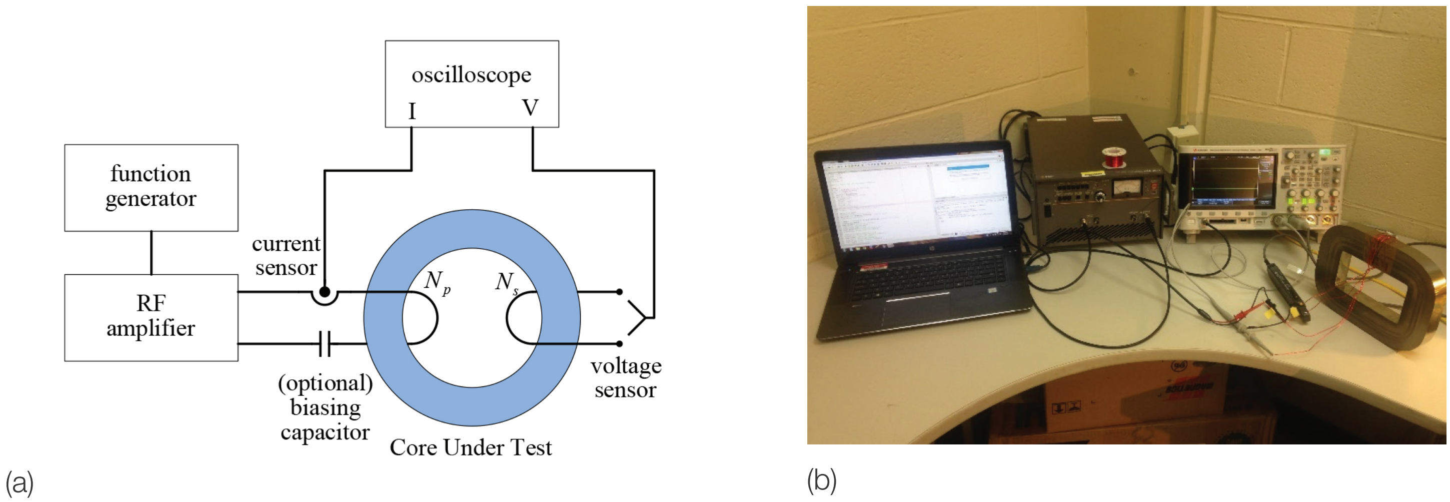


*Fig. 3: Arbitrary waveform core loss test system (CLTS) (a) conceptual setup (b) actual setup.*

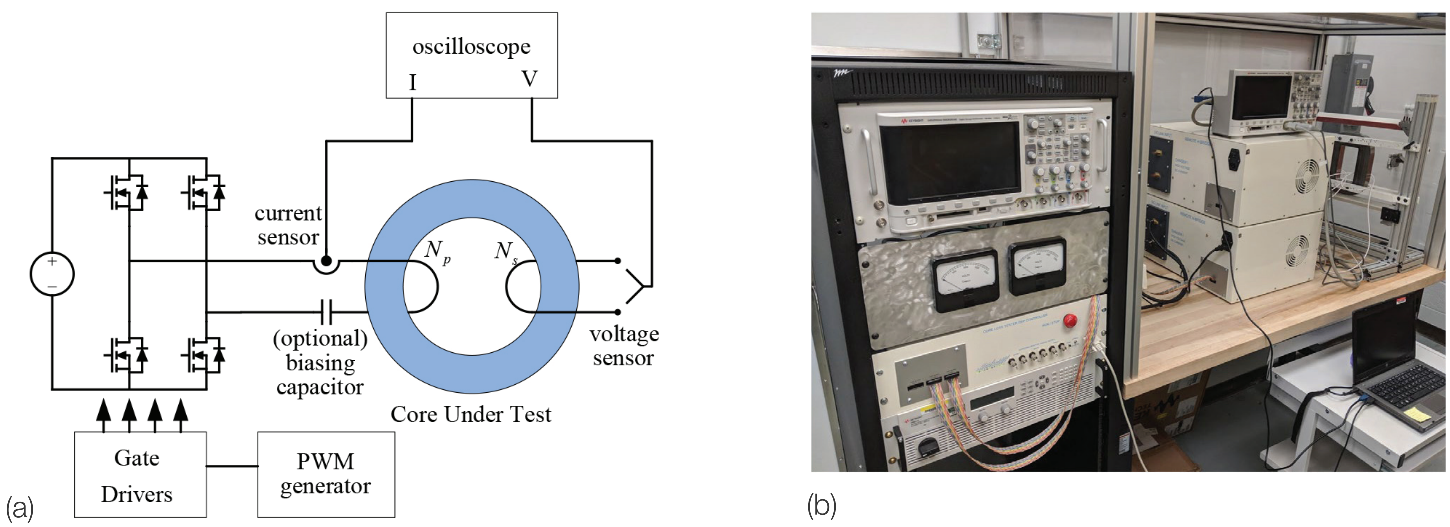


*Fig. 4: Square waveform core loss test system (CLTS) (a) conceptual setup (b) actual setup.*

---

[1] Mean magnetic path length is computed using the following equation. OD and ID are outer and inner diameters, respectively. $L_m = \dfrac{\pi(\mathrm{OD}-\mathrm{ID})}{\ln\left(\dfrac{\mathrm{OD}}{\mathrm{ID}}\right)}$

Arbitrary and square waveform core loss test systems (CLTS) are utilized to characterize soft magnetic materials, which are shown in Fig. 3 and Fig. 4, respectively. Fig. 5 illustrates three different excitation voltage waveforms and corresponding flux density waveforms. In the arbitrary waveform CLTS, a function generator generates any arbitrary small signal, and the small signal is amplified and applied to a core under test (CUT) using a linear amplifier. The arbitrary waveform CLTS is advantageous in that any waveforms can be easily applied to characterize a CUT; however, the linear amplifier has limited electrical capabilities, such as ±75V & ±6A peak ratings and 400V/µs slew rate. Therefore, a full core characterization may not be possible in some cases, such as low permeability cores, high frequency, and/or large sized cores. The arbitrary waveform CLTS is utilized to perform sinusoidal waveform measurements, as shown in Fig. 5(a). The square waveform CLTS is utilized to perform various square waveform measurements with different duty cycles, as shown in Fig. 5(b) and (c). 1200V SiC MOSFET devices are utilized to extend the core characterization range.

Two windings are placed around the core under test. The amplifier excites the primary winding, and the current of the primary winding is measured, in which the current information is converted to the magnetic field strengths $H$ as

$$H(t) = \frac{N_p \cdot i(t)}{l_m}, \qquad (1)$$

where $N_p$ is the number of turns in the primary winding. A dc-biasing capacitor is inserted in series with the primary winding to provide zero average voltage applied to the primary winding.

The secondary winding is open, the voltage across the secondary winding is measured, in which the voltage information is integrated to derive the flux density $B$ as

$$B(t) = \frac{1}{N_s \cdot A_e} \int_0^T v(\tau)\, d\tau, \qquad (2)$$

where $N_s$ is the number of turns in the secondary winding, and $T$ is the period of the excitation waveform.

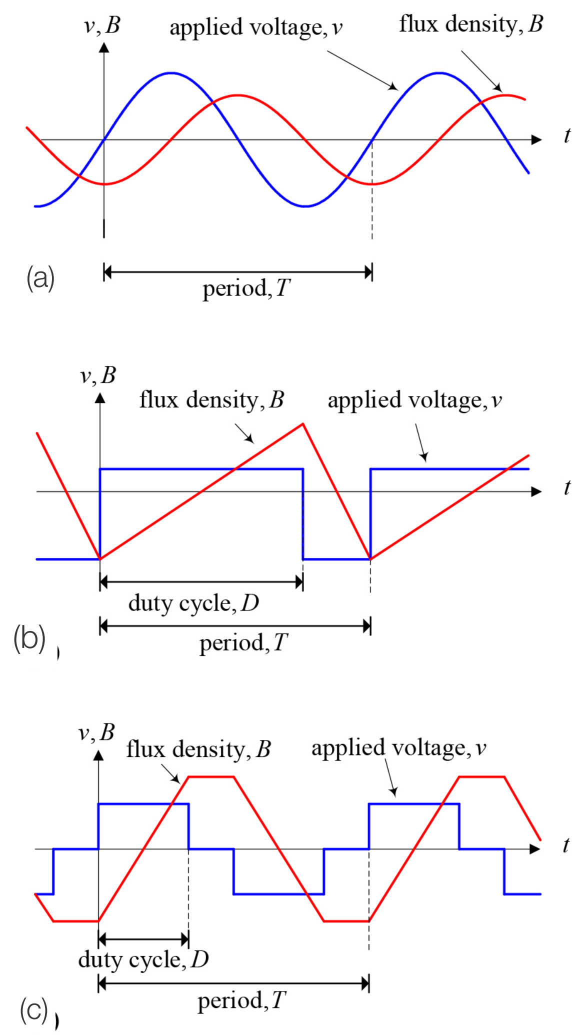

*Fig. 5: Excitation voltage waveforms and corresponding flux density waveforms (a) Sinusoidal excitation with sinusoidal flux, (b) Asymmetrical excitation with sawtooth flux, and (c) Symmetrical excitation with trapezoidal flux.*

In Fig. 5(a), the excitation voltage is sinusoidal, and its flux waveform is also a sinusoidal shape. In Fig. 5(b), the excitation voltage is a two-level square waveform with asymmetrical duty cycle between high-level and low-level voltages, and its flux waveform is a sawtooth shape. It is hereafter referred as asymmetrical waveform. Its duty cycle is defined as the ratio between the applied high voltage time and the period, and the duty cycle can range from 0% to 100%. Furthermore, the average excitation voltage is adjusted to be zero via the dc-biasing capacitor, and thus, the average flux is also zero. In Fig. 5 (c), the excitation voltage is a three-level square voltage with symmetrical duty cycle between high-level and low-level voltages, and its flux waveform is a trapezoidal shape. It is hereafter referred as symmetrical waveforms. Its duty cycle is defined as the ratio between the applied high-level voltage time and the period, and the duty cycle can range from 0% to 50%. At 50% duty cycles, both the asymmetrical and symmetrical waveforms become identical.

## Core Losses

Core losses at various frequencies and induction levels are measured using various excitation waveforms. Based on measurements, the coefficients of the Steinmetz's equation are estimated. The Steinmetz's equation is given as

$$P_w = k_w \cdot \left( f / f_0 \right)^{\alpha} \cdot \left( B / B_0 \right)^{\beta} \quad , \tag{3}$$

where $P_w$ is the core loss per unit weight, $f_0$ is the base frequency, $B_0$ is the base flux density, and $k_w$, $\alpha$, and $\beta$ are the Steinmetz coefficients from empirical data. In the computation of $P_w$, the weight before impregnation in Table 2 is used, the base frequency $f_0$ is 1 Hz, and the base flux density $B_0$ is 1 Tesla.

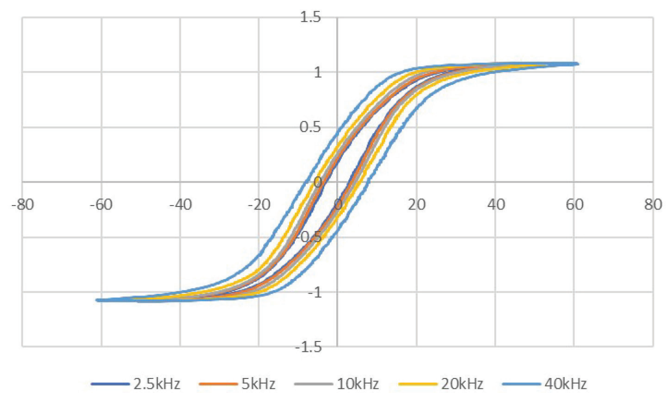


*Fig. 6: BH curve as a function of frequency.*

Fig. 6 illustrates the measured BH curve at different frequencies. The field strength $H$ is kept near constant for all frequency. At 2.5 kHz and 5 kHz excitations, the BH curve is similar, which indicates that the hysteretic losses are the dominant factor at frequencies below 2.5 kHz. As frequency increases, the BH curves become thicker, which indicates that the eddy current and anomalous losses are becoming larger.

*Table 3: Empirical Steinmetz coefficients.*

| | $k_w$ | *A* | $\beta$ |
|---|---|---|---|
| sine | 1.85585398850933e-05 | 1.49277818956666 | 2.27139341936170 |
| Square 50% duty | 5.36229287071411e-06 | 1.61360755255344 | 2.98478154030210 |
| Asymmetrical 40% duty | 4.87862939522679e-06 | 1.62644460441331 | 3.07544542555101 |
| Asymmetrical 30% duty | 3.81431022346796e-06 | 1.65951366804733 | 3.17550540860410 |
| Asymmetrical 20% duty | 2.84050228665688e-06 | 1.70698527974095 | 3.12352530698320 |
| Asymmetrical 10% duty | 2.55230135725345e-06 | 1.75926006495231 | 2.74704211304795 |
| Symmetrical 40% duty | 5.37045792478309e-06 | 1.63427405423232 | 2.89718665363610 |
| Symmetrical 30% duty | 4.71314135150713e-06 | 1.66524372330867 | 2.65300084648117 |
| Symmetrical 20% duty | 3.95961815205635e-06 | 1.71006588409068 | 2.57611899068625 |
| Symmetrical 10% duty | 6.32748185119464e-06 | 1.71030804680467 | 2.35347191564708 |

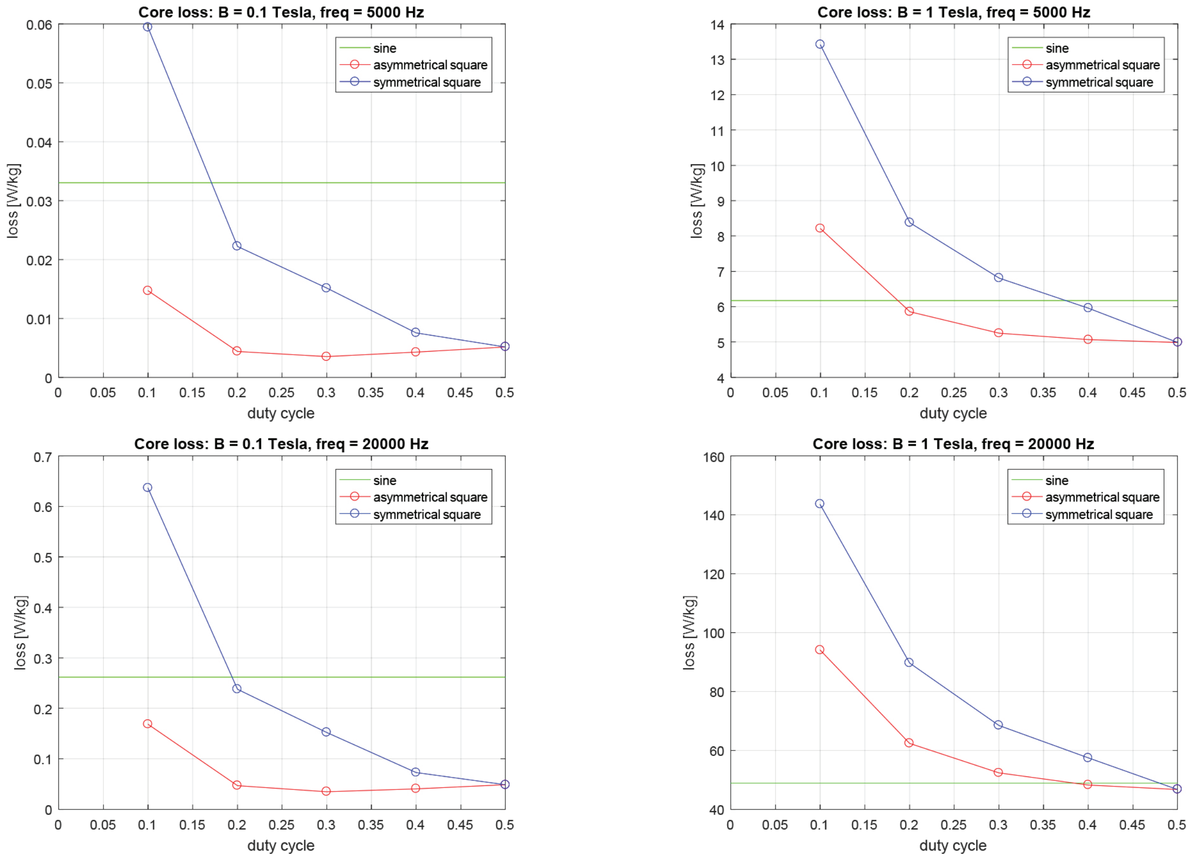


*Fig. 7: Estimated core losses of sine and square excitation at various flux density, frequency, and duty cycle.*

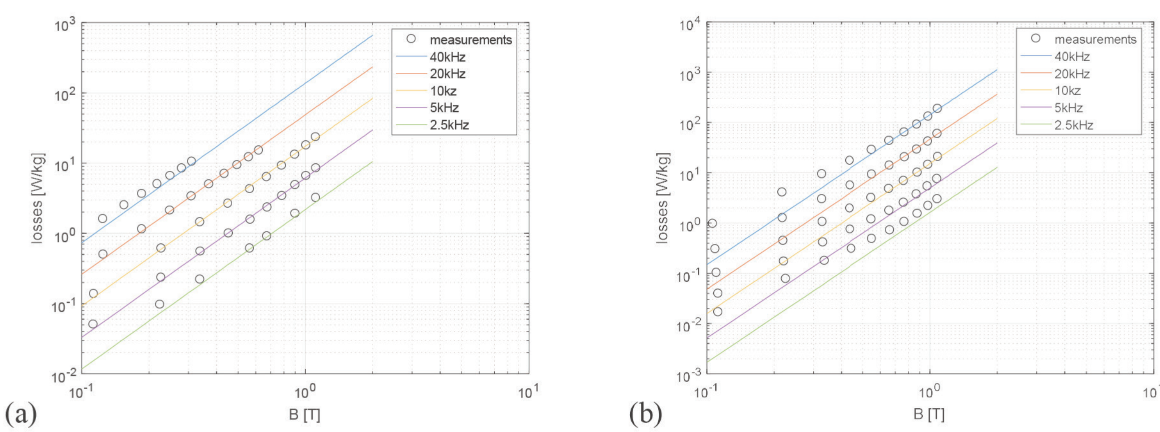


*Fig. 8: Core loss measurements and estimations via Steinmetz equation: (a) Sine (b) Square at 50% duty.*

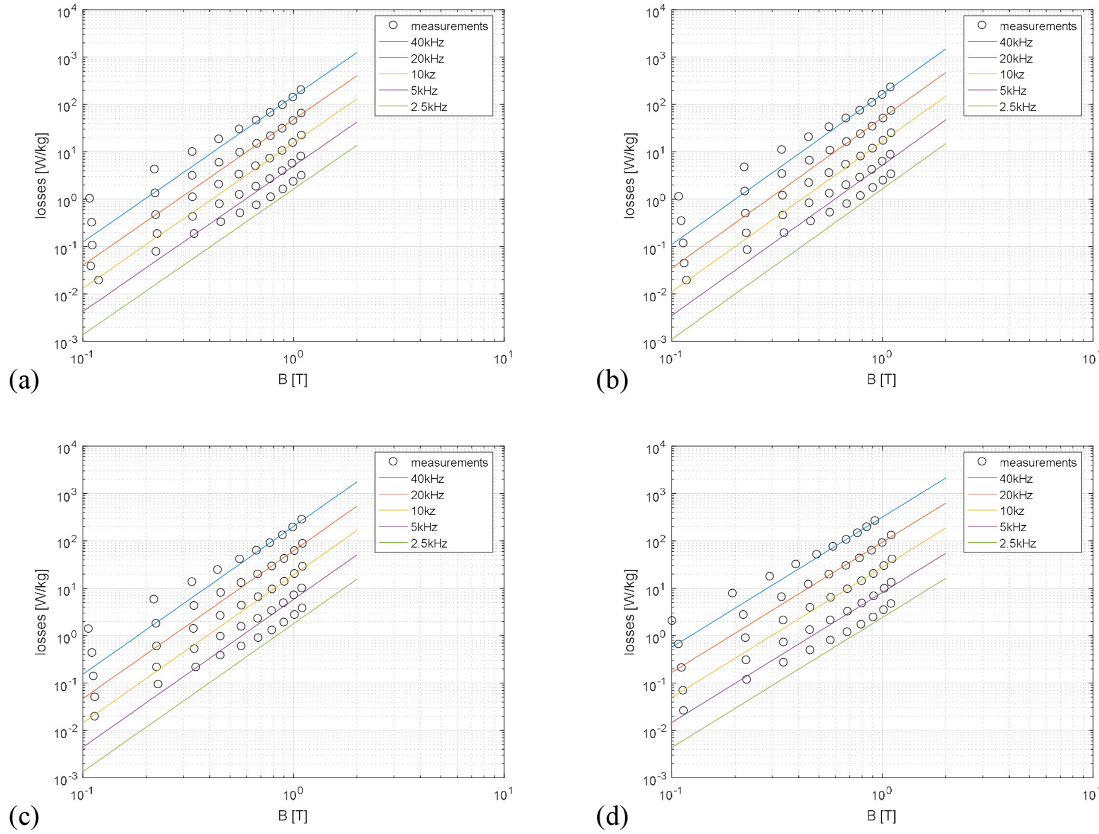


*Fig. 9: Core loss measurements and estimations via Steinmetz equation of asymmetrical square waveform excitation: (a) 40% duty (b) 30% duty (c) 20% duty (d) 10% duty.*

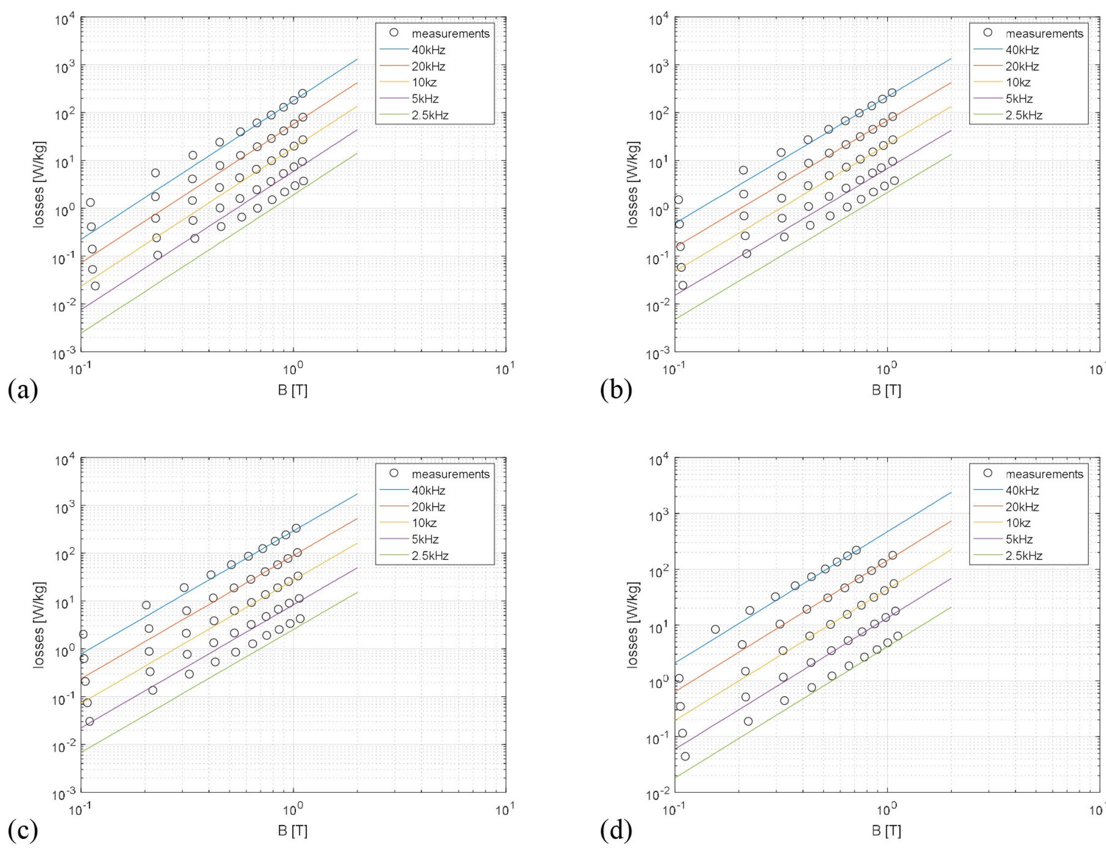


*Fig. 10: Core loss measurements and estimations via Steinmetz equation of symmetrical square waveform excitation: (a) 40% duty (b) 30% duty (c) 20% duty (d) 10% duty.*

Table 3 lists the Steinmetz coefficients at different excitation conditions.

Fig. 7 illustrates estimated core losses of sine and square excitation at various flux density, frequency, and duty cycle based on the empirical Steinmetz coefficients in Table 3.

Fig. 8, Fig. 9, and Fig. 10 illustrate the core loss measurements data points and estimations via Steinmetz equation of sine, asymmetrical, and symmetrical square excitation waveforms at various duty cycles.

## Core Permeability

The permeability of the core is measured as functions of flux density and frequency. Following figures illustrate the measured absolute relative permeability $\mu_r$ values, which is defined as

$$\mu_r = \frac{B_{peak}}{\mu_0 \cdot H_{peak}} \tag{4}$$

where $B_{peak}$ and $H_{peak}$ are the maximum flux density and field strength at each measurement point. Under certain excitation conditions, the core could not be saturated due to lack of available voltages. For example, the sine excitation is performed using the arbitrary CLTS, and its voltage is limited to ±75V. Furthermore, the square CLTS could not saturate the core during the highest frequency and 10% duty cycle.

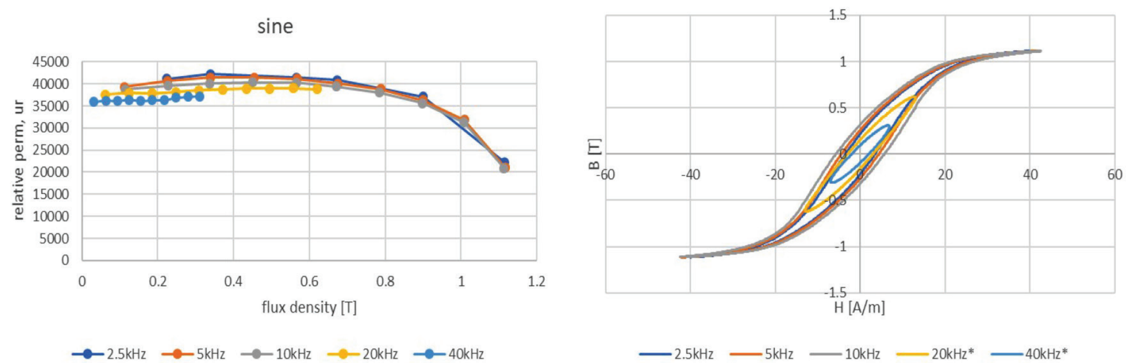


*Fig. 11 Sinusoidal excitation: relative permeability as a function of flux density and frequency (left column) and BH loop at the maximum B of the corresponding frequency (right column) (* could not saturate the core under the condition).*

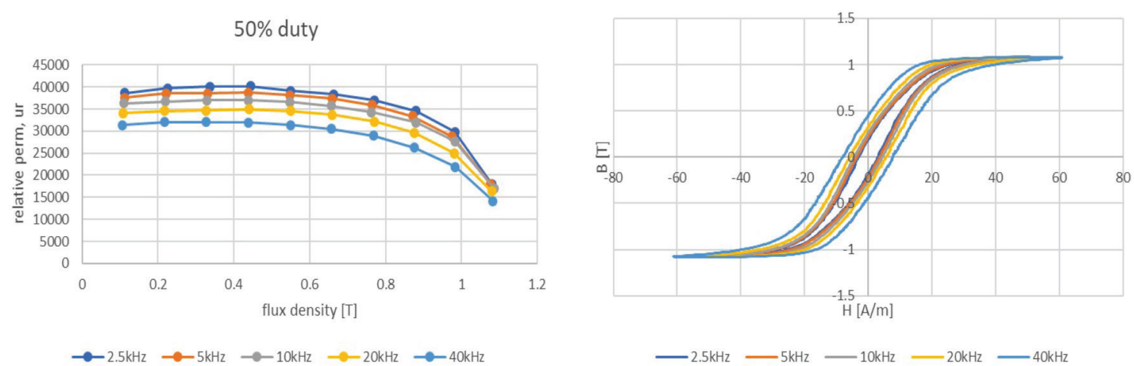


*Fig. 12: Square excitation with 50% duty cycle: relative permeability as a function of flux density and frequency (left column) and BH loop at the maximum B of the corresponding frequency (right column).*

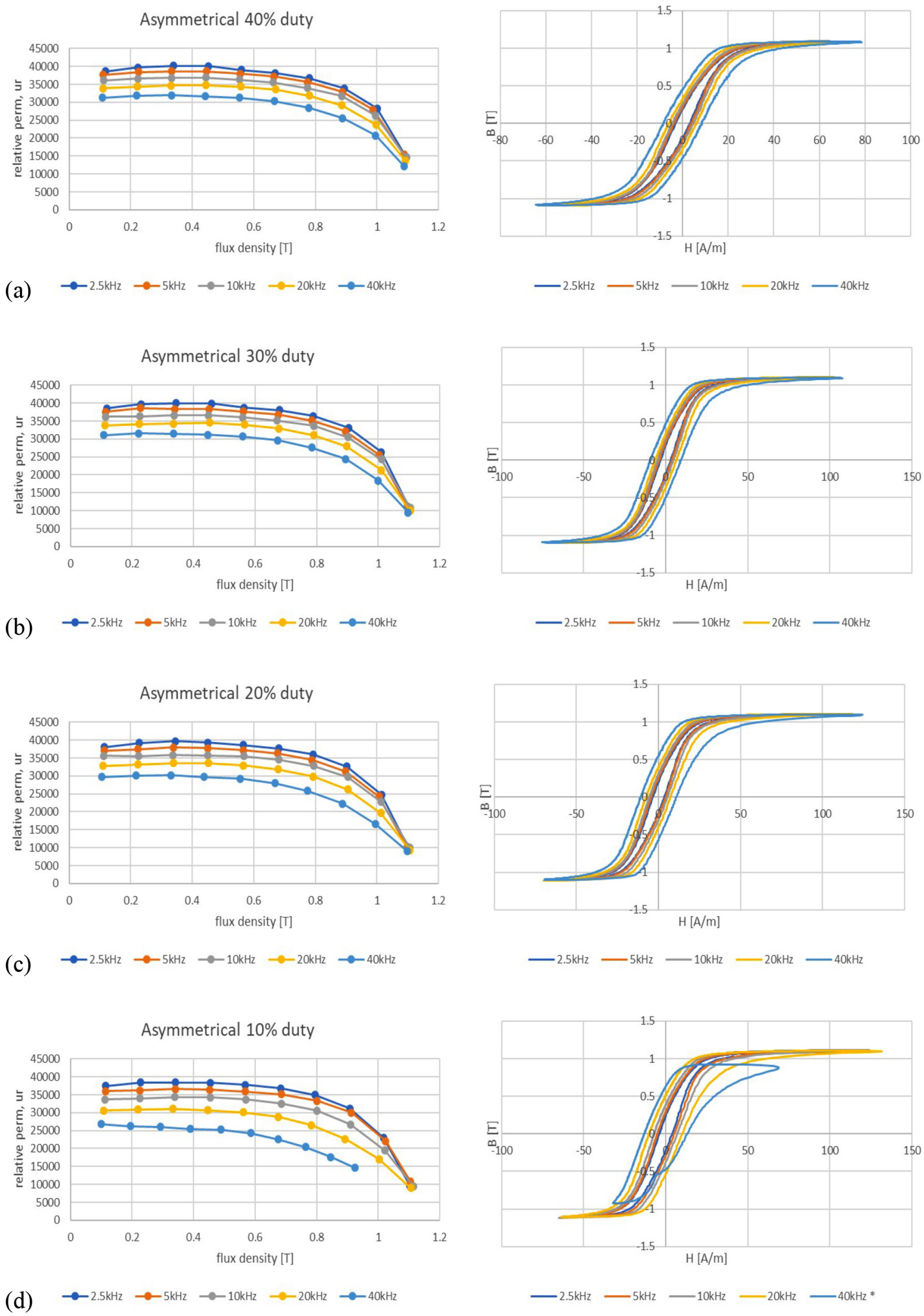


*Fig. 13: Asymmetrical excitation with various duty cycle: relative permeability as a function of flux density and frequency (left column) and BH loop at the maximum B of the corresponding frequency (right column) (a) 40% duty (b) 30% duty (c) 20% duty (d) 10% duty (* could not saturate the core under the condition).*

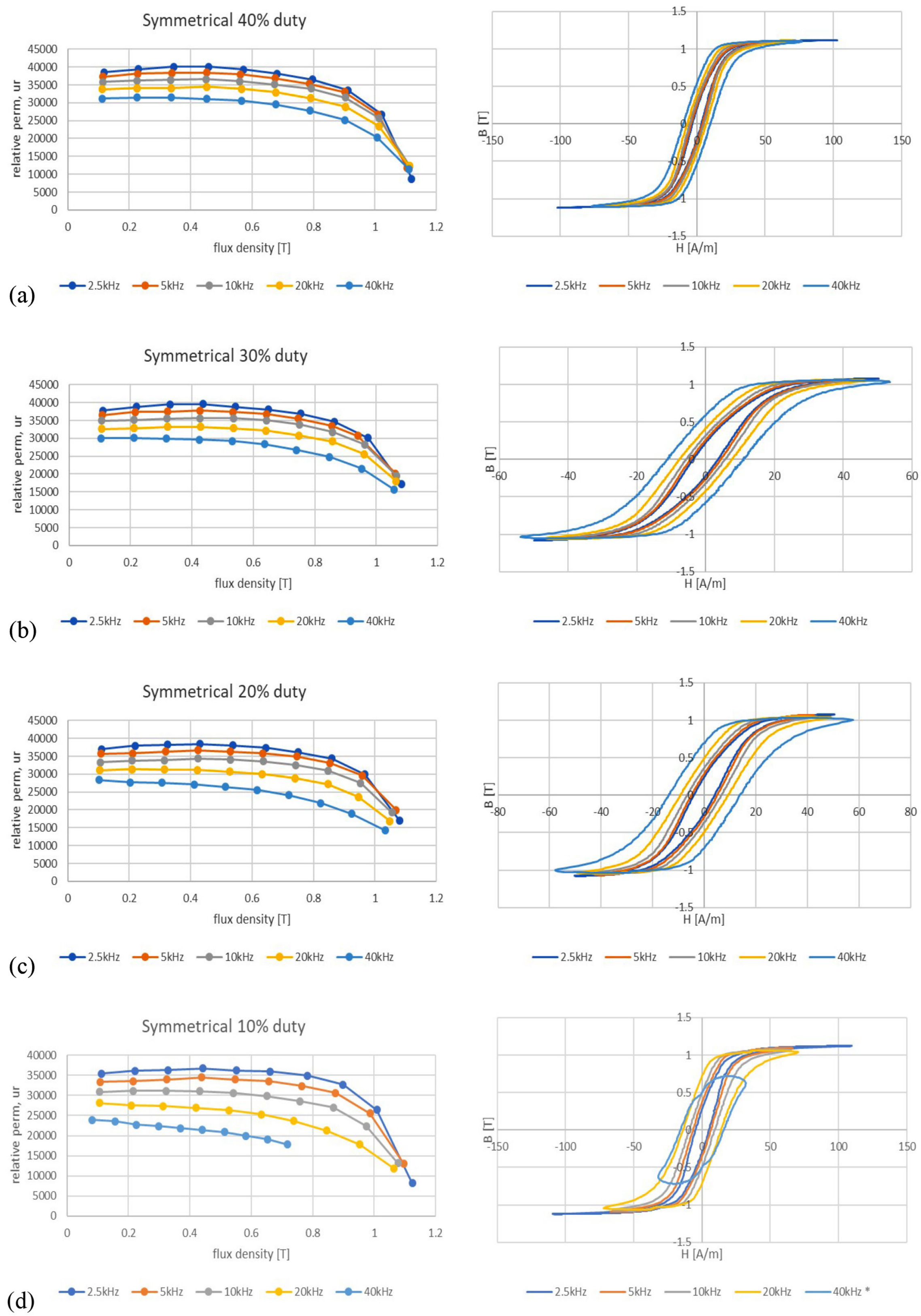


*Fig. 14: Symmetrical excitation with various duty cycle: relative permeability as a function of flux density and frequency (left column) and BH loop at the maximum B of the corresponding frequency (right column) (a) 40% duty (b) 30% duty (c) 20% duty (d) 10% duty (* could not saturate the core under the condition).*

## Anhysteretic BH Curves

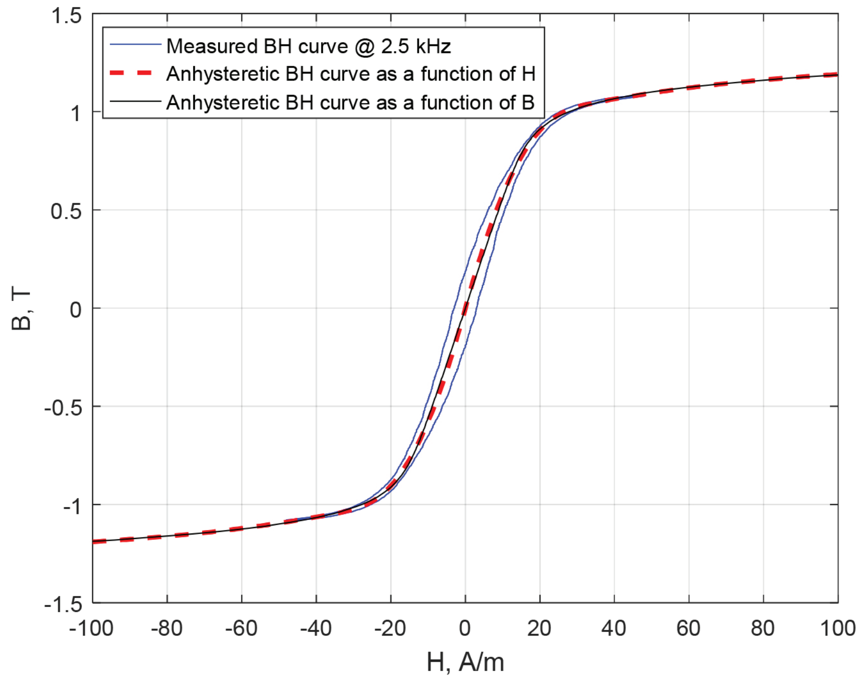


*Fig. 15: Measured BH curve and fitted anhysteretic BH curve as functions of H and B*

*Table 4: Anhysteretic curve coefficients for B as a function of H.*

| $k$ | 1 | 2 | 3 | 4 |
|---|---|---|---|---|
| $m_k$ | 1.36188609252256 | 0.765618320366765 | -0.0792251538183330 | 0.189040210158061 |
| $h_k$ | 39.2995499730024 | 24.8042861895068 | 30.4180850122747 | 28.1487359089928 |
| $n_k$ | 1 | 1.69418036742318 | 1.10000000913635 | 4.87069364694230 |

*Table 5: Anhysteretic curve coefficients for H as a function of B.*

| $k$ | 1 | 2 | 3 | 4 |
|---|---|---|---|---|
| $\mu_r$ | 45064.6754381427 | | | |
| $\alpha_k$ | 0.687889508419379 | 0.0322172218029199 | 0.00434791130291862 | 0.00100000044145802 |
| $\beta_k$ | 289.721398457367 | 66.2809626520291 | 11.0711903781493 | 4.21749966103008 |
| $\gamma_k$ | 1.32510736741664 | 1.30748851999270 | 1.32215018640792 | 2.14652639674268 |
| $\delta_k$ | 0.00237431377896860 | 0.000486070517292549 | 0.000392723018429880 | 0.000237107414778968 |
| $\varepsilon_k$ | 1.85846510725429e-167 | 2.30858728422451e-38 | 4.39434632822357e-07 | 0.000117028696243744 |
| $\zeta_k$ | 1 | 1 | 0.999999560565367 | 0.999882971303756 |

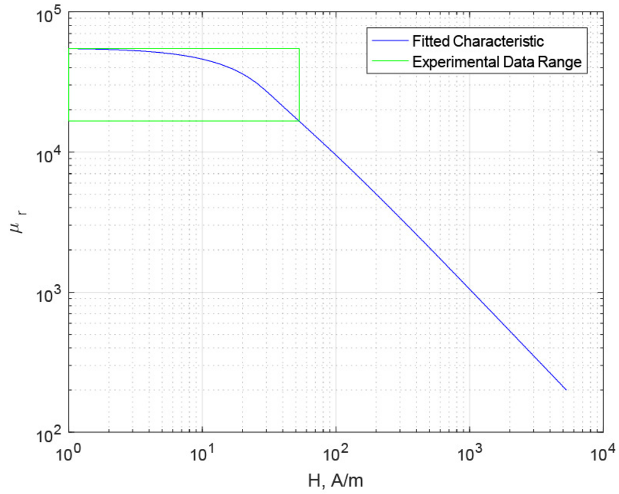


*Fig. 16: Absolute relative permeability as function of field strength H.*

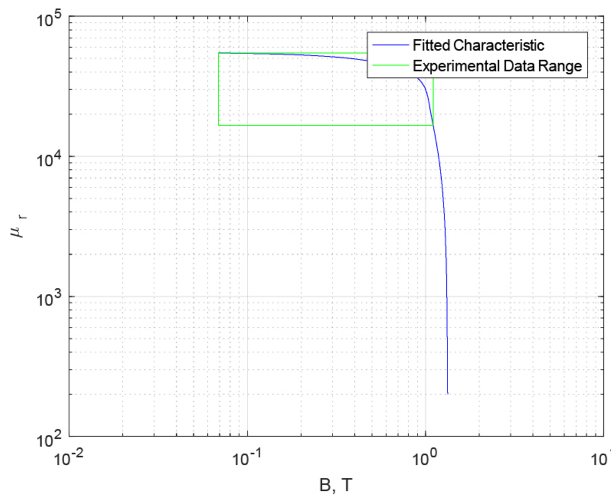


*Fig. 17: Absolute relative permeability as function of flux density B.*

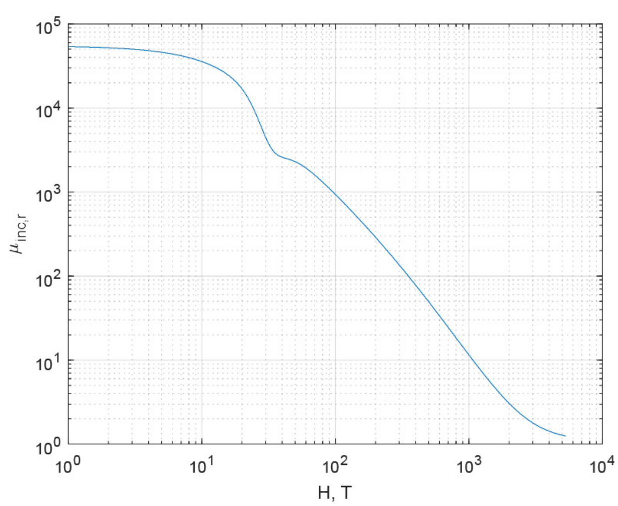


*Fig. 18: Incremental relative permeability.*

Fig. 15 illustrates the measured BH curve and fitted anhysteretic BH curves as functions of $H$ and $B$. The anhysteretic BH curves can be computed as a function of field intensity $H$ using the follow formula.

$$B = \mu_H(H)H$$
$$\mu_H(H) = \mu_0 + \sum_{k=1}^{K} \frac{m_k}{h_k} \frac{1}{1+\left|H/h_k\right|^{n_k}} \tag{5}$$

Similarly, the anhysteretic BH curves can be computed as a function of flux density $B$ using the follow formula.

$$B = \mu_B(B)H$$
$$\mu_B(B) = \mu_0 \frac{r(B)}{r(B)-1}$$
$$r(B) = \frac{\mu_r}{\mu_r - 1} + \sum_{k=1}^{K} \alpha_k |B| + \delta_k \ln\left(\varepsilon_k + \zeta_k e^{-\beta_k |B|}\right) \tag{6}$$
$$\delta_k = \frac{\alpha_k}{\beta_k}, \varepsilon_k = \frac{e^{-\beta_k \gamma_k}}{1+e^{-\beta_k \gamma_k}}, \zeta_k = \frac{1}{1+e^{-\beta_k \gamma_k}}$$

Table 4 and Table 5 lists the anhysteretic curve coefficients for eqs. (5) and (6), respectively.

The core anhysteretic characteristic models in eqs. (5) and (6) are based on the following references.

Scott D. Sudhoff, “Magnetics and Magnetic Equivalent Circuits,” in *Power Magnetic Devices: A Multi-Objective Design Approach*, 1, Wiley-IEEE Press, 2014, pp.488-

G. M. Shane and S. D. Sudhoff, “Refinements in Anhysteretic Characterization and Permeability Modeling,” in *IEEE Transactions on Magnetics*, vol. 46, no. 11, pp. 3834-3843, Nov. 2010.

The estimation of the anhysteretic characteristic is performed using a genetic optimization program, which can be found in the following websites:

https://engineering.purdue.edu/ECE/Research/Areas/PEDS/go_system_engineering_toolbox

## Core Characteristic Variation as a Function of Temperature

At this time, the core temperature is not monitored, and this version of data sheet does not have this information. However, in future editions, it is planned to be included.